IEEE Access
Multidisciplinary ⋮ Rapid Review ⋮ Open Access Journal

Received 1 January 2023, accepted 11 January 2023, date of publication 20 January 2023, date of current version 3 February 2023.

Digital Object Identifier 10.1109/ACCESS.2023.3238335

RESEARCH ARTICLE

Performance Analysis of NOMA-Based Hybrid Satellite-Terrestrial Relay System Using mmWave Technology

NHAT-TIEN NGUYEN[1,2], HONG-NHU NGUYEN[2], NGOC-LONG NGUYEN[3], ANH-TU LE[4], (Member, IEEE), TAN N. NGUYEN[5], (Member, IEEE), AND MIROSLAV VOZNAK[1], (Senior Member, IEEE)

[1]Faculty of Electrical Engineering and Computer Science, VSB–Technical University of Ostrava, 70800 Ostrava, Czech Republic
[2]Faculty of Electronics and Telecommunications, Saigon University (SGU), Ho Chi Minh City 700000, Vietnam
[3]Faculty of Applied Sciences, Ton Duc Thang University, Ho Chi Minh City 70000, Vietnam
[4]Faculty of Electrical and Electronics Engineering, Ton Duc Thang University, Ho Chi Minh City 70000, Vietnam
[5]Communication and Signal Processing Research Group, Faculty of Electrical and Electronics Engineering, Ton Duc Thang University, Ho Chi Minh City 70000, Vietnam

Corresponding author: Tan N. Nguyen (nguyennhattan@tdtu.edu.vn)

This work was supported in part by the Ministry of Education, Youth and Sports of the Czech Republic under Grant SP2022/5; and in part by e-INFRA CZ under Grant 90140.

ABSTRACT This paper investigates the performance of NOMA-based hybrid Satellite-Terrestrial relays system (HSTR) using the millimeter wave (mmWave) technology. Furthermore, the relays are equipped with multiple antennas and utilize the amplify and forward (AF) protocol to forward the satellite's superimposed information to multiple destinations. Then, the rain coefficient is considered as the fading factor of the mmWave band to choose the best relay. We considered the shadowed-Rician fading and Nakagami-m fading for satellite links and terrestrial links respectively, and in addition, we evaluated the shadowing effect for satellite links with two modes of: frequent heavy shadowing (FHS) and average shadowing (AS). With these suggestions, the closed-form outage probability (OP) and approximate ergodic capacity (EC) are derived to evaluate the efficiency of the proposed system. Next contribution of the research is an asymptotic analysis for the OP, which is derived in order to gain additional insight into important system parameters. Finally, the theoretical derivation is validated through simulation results and analyzed the impact of significant parameters. These results demonstrate NOMA's superiority to the traditional orthogonal multiple access (OMA) method in the proposed system.

INDEX TERMS NOMA, hybrid satellite-terrestrial relay system, millimeter wave, rain attenuation, outage probability, ergodic capacity.

I. INTRODUCTION

Recently, satellite communication (SatCom) has been one of the potential technologies for the fifth generation (5G) network and beyond, which brings many advantages such as high throughput, great reliability, extensive coverage, inexpensive operations, and energy-efficient [1], [2], [3]. Therefore, the integration of SatCom into current terrestrial communication systems has received considerable attention in researching and proposing models of the integrated satellite terrestrial network (ISTN) [4], [5]. In SatCom, geostationary Earth orbit (GEO), middle Earth orbit (MEO), and low Earth orbit (LEO) satellites can operate efficiently in the high frequency bands of millimeter wave (mmWave) (e.g. Ka/Q/V-band) [6]. They effectively provide system throughput and extensive coverage of the terrestrial wireless network [7], [8]. However, using the traditional orthogonal multiple access (OMA) technique into SatCom would result in a waste of block resources, such as the time / frequency / code block due to the limitation in the number of simultaneously

The associate editor coordinating the review of this manuscript and approving it for publication was Abdel-Hamid Soliman.

connected users, the ability to meet for the services requires low latency and high throughput [9], [10]. Contributing to solving the limitations of OMA, a promising technology has been proposed for 5G is non-orthogonal multiple access (NOMA) [11]. NOMA helps improve resource efficiency and increase the number of users served in the same resource block with higher data speed, higher reliability, and lower latency than the conventional OMA scheme [12]. With these advantages, the combination of SatCom with NOMA will greatly improve network performance; therefore, this is a promising job in the future.

A. RELATE WORK

Under the influence of rain, fog, and obstacles, the performance of ground users will be severely affected. Therefore, the hybrid satellite-terrestrial relay network (HSTRN) is proposed to solve the above problems. The authors in [13] presented the relay selection as well as round-robin scheduling schemes for the physical-layer security (PLS) in HSTRN, where secrecy performance has been analyzed with the decode and forward (DF) relaying protocol. To evaluate the security and reliability for a satellite-terrestrial network with multiple ground relays in the presence of an eavesdropper, the authors in [14] deployed a friendly jammer and an amplify-and-forward based relaying scheme to subtract the consequence of the eavesdropper on system performance. In [15], the authors investigated the ergodic capacity (EC) in HSTRN with adopted amplify-and-forward (AF) relaying protocol. Furthermore, the authors combined opportunistic scheduling for terrestrial destinations. To achieve optimal power performance, rate adaptation and truncated channel inversion with fixed rate in HSTRN have been proposed in [16]. In [17], the authors employed a cache-enabled for HSTRN, which is regarded as the common and most widely used content-based caching strategy. The average symbol error rate (ASER) has been examined in both cases of a degraded LoS link and without a degraded LoS link are presented in [18] and [19] respectively. The authors in [20] analyzed the OP performance of decode-and-forward HSTRN with the best relay selection technique while taking into account a multiple-relay scenario. Also, the performance of downlink HSTRN with relay selection was presented in [21]. Furthermore, hardware impairments (HIs) and interference are considered for the relay and terrestrial destination. The effect of co-channel interference (CCI) in HSTRN has been evaluated in terms of bit error rate at the relay and destination nodes in [22]. To increase the total throughput and reduce system complexity, full-duplex (FD) and relay selection techniques are applied at the relay proposed in [23].

The NOMA scheme is considered to improve spectrum efficiency and serve multiple users in a time/frequency/code block in conjunction with HSTRN. Recently, the investigations on the impact of NOMA on satellite-terrestrial network (STN) in order to use spectrum efficiently and serve multiple users at the block resources [24], [25], [26], [27]. The exact outage behaviors of NOMA-based STN and asymptotic analysis were studied by the authors in [24]. The identical OP analysis was achieved in [25], where the authors discussed the effectiveness of the NOMA-based uplink land mobile satellite (LMS) communications. The authors in [26] considered the outage probability (OP) and asymptotic OP obtained after evaluating the system performance of NOMA-based HSTRN with the AF protocol. To maximize the sum rate of the suggested NOMA-based HSTRN, the authors provided an iterative penalty function based beamforming (BF) method. This algorithm could quickly get the BF weight vector and power coefficient [27]. In order to collaborate with the primary satellite network for dynamic spectrum access, the secondary terrestrial network and overlay cognitive integrated satellite-terrestrial relay network (CISTRN) based on NOMA were examined in [28] and [29]. Moreover, the authors in [30] analyzed the performance of the secondary network when the near user employed the full-duplex mode and used the DF protocol to enhance the performance of far user in NOMA network. In [31], the authors investigated the OP and average transit time for an underlay cognitive NOMA-based HSTRN with a HD secondary receive. Table 1 summarized the related work on NOMA-based Satellite network, in which their features, Methodology and challenges are highlighted to previous works.

B. MOTIVATIONS AND CONTRIBUTIONS

To the best of our knowledge, the NOMA-based HSTRN with mmWave network has not yet been disclosed. And this paper is an expansion of [6], [28], and [37]. In particular, the following can be summarized as our significant contributions.

- First, we proposed a NOMA-based HSTRN with mmWave network, where a GEO satellite and AF protocol relaying are considered. Furthermore, we investigate the rain attenuation values to select the desired transition node. In addition, we consider the multi-device serving model in NOMA to improve the spectrum.
- Second, we analyze the performance of the system based on the channel fading distribution. The closed-form OP and EC are expressed. To obtain the insights, the asymptotic OP and diversity are derived for the system. To further confirm the accuracy of our findings, Monte Carlo (MC) simulations are presented.
- Finally, we consider the effects of key parameters on the proposed system. Additionally, the benchmarks for comparing the NOMA-based scheme to the OMA-based scheme are supplied, demonstrating the benefits of the NOMA scheme.

The rest of this paper is organized as follows. Section II introduces the proposed system model, the type of satellite, and received SINR. In Section III, the channel model is introduced. Section IV, the closed-form OP, EC, and diversity order are derived. The simulation results are shown in Section IV. In Section V, conclusions are reached.

II. SYSTEM MODEL

In this paper, we consider an AF-multirelay satellite cooperative NOMA network as shown in Fig. 1, which

TABLE 1. Features, methodology and challenges of previous works on NOMA-based Satellite Networks.

Papers (years)	Features	Methodology	Challenges
[21] (2020)	MIMO-DF relay protocol, relay selection and GEO satellite	Outage probability, throughput of system and asymptotic outage are analyzed	Without NOMA, low frequency
[32] (2020)	Satellite network cooperative with NOMA	Outage probability and asymptotic outage are analyzed	Without relay, two destinations, low frequency
[33] (2021)	DF MIMO relay protocol, cooperative with NOMA	Outage probability and asymptotic outage are analyzed	Two destinations, low frequency
[34] (2021)	DF relay protocol, relay selection, GEO satellite, satellite network cooperative with NOMA	Outage probability, asymptotic outage and ergodic capacity are analysis	Two destinations, single antenna at relay, low frequency
[35] (2022)	DF relay protocol, relay selection, LEO satellite, cooperative with NOMA	Outage probability and asymptotic outage are analyzed	Two destinations, low frequency, single antenna at relay
[36] (2022)	AF relay protocol, Multiple destinations, GEO satellite, cooperative with NOMA	Outage probability and asymptotic outage are analyzed	Single relay, low frequency, single antenna at relay

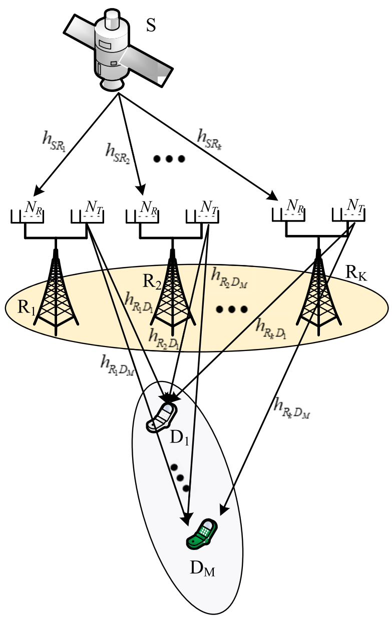

FIGURE 1. System model of Satellite in mmWave networks.

consists of the source node S, the K terrestrial relay nodes $R_k(k = 1, 2, \ldots, K)$ equipped with N_R receiving antennas and N_T transmitting antennas, and M devices $D_m(m = 1, 2, \ldots, M)$. Furthermore, we assume that the direct communication links between S and D_m are not available due to the heavy shadowing [38]. Therefore, satellite S communicates with the terrestrial devices with the help of the best terrestrial relay R_{k*} based on opportunistic scheduling [6].

In the first phase, the satellite transmits the signal $x_S = \sum_{i=1}^{M} \sqrt{\varpi_i} x_i$ to the relay node R_{k*}, and the relay node performs the maximum ratio combining (MRC) to combine the received signals [39]. Hence, the received signal at the best relay node is given by

$$\begin{aligned} y_{SR_{k*}} &= \sqrt{L_S G_S(\phi) G_R P_S}\,\vartheta_{r,k*} \mathbf{h}_{SR_{k*}} \mathbf{w}_{SR_{k*}}^H x_S + n_{R_{k*}} \\ &= \sqrt{L_S G_S(\phi) G_R P_S}\,\vartheta_{r,k*} \mathbf{h}_{SR_{k*}} \mathbf{w}_{SR_{k*}}^H \sum_{i=1}^{M} \varpi_i x_i + n_{R_{k*}} \end{aligned} \quad (1)$$

TABLE 2. The table of main notication.

Notation	Definition
K	Number of relays
M	Number of Devices
N_R	Number received antenna of relays
N_T	Number transmit antenna of relays
P_S	Transmit power of satellite
P_R	Transmit power of relays
x_i	The signal of D_i
ϖ_i	The power allocation
$\vartheta_{r,k*}$	The expected rain attenuation of link from S to R_{k*}
$\vartheta_{d,m*}$	The expected rain attenuation of link from R_{k*} to devices D_m
G_S	The antenna gain at the satellite
$G_R^{\max}$	The antenna gain at relays
$(\bullet)^H$	The Hermitian transpose
$\|\| \bullet \|\|_F$	The Frobenius norm
$J_\nu(\bullet)$	The first-kind Bessel function with order ν
$\mathcal{B}(\bullet, \bullet)$	The Beta function
$\gamma(\bullet, \bullet)$	The lower incomplete gamma function
$K_\nu(\bullet)$	The second-kind Bessel function with order ν

where $\mathbf{h}_{SR_{k*}} = [h_{SR_{k*}}^1, h_{SR_{k*}}^2, \ldots, h_{SR_{k*}}^{N_R}]^T$ is the $N_R \times 1$ channel coefficient vector between S and R_{k*}, $\vartheta_{r,k*}$ denote the expected rain attenuation between S and R_{k*}, $\mathbf{w}_{SR_{k*}} = \frac{\mathbf{h}_{SR_{k*}}}{||\mathbf{h}_{SR_{k*}}||_F}$ is the receive beamforming weight vector and $n_{R_{k*}}$ is the vector of zero mean additive white Gaussian noise (AWGN) with variance N_0. Then the desired relay node amplifies the received signal $y_{SR_{k*}}$ by a gain factor $G = \sqrt{\frac{1}{P_S \|\mathbf{h}_{SR_{k*}}\|_F^2 \vartheta_{r,k}^2 + N_0}}$, and performs maximum ratio transmission (MRT) to forward it to the desired destination node according to the feedback of pilot signal from each destination node during second phase [39]. Additionally, the free space pathloss coefficient L_S can be expressed as [34], [40], and [31]

$$L_S = \frac{\lambda^2}{(4\pi d_R)^2 N_p} \quad (2)$$

where $\lambda = \frac{c}{f_c}$ is the wavelength, c is the light speed, f_c is the carrier frequency, d_R is the distance between the satellite and R_{k*}, $N_p = K_B T B_\omega$ is noise power, K_B denote the Boltzmann constant, T is the noise temperature of the terrestrial receiver and B_ω represents the bandwidth. For the R_{k*} location, ϕ represents the angle between R_{k*} and beam center compared to the satellite. In addition, G_R denotes the antenna gain at R_{k*}, $G_S(\phi)$ denotes the satellite beam gain, and the beam gain $G_S(\phi)$ is given as [34]

$$G_S(\phi) = G_S^{\max}\left(\frac{J_1(u)}{2u} + 36\frac{J_3(u)}{u^3}\right)^2 \tag{3}$$

where $G_S^{\max}$ denotes the maximal beam gain and u can be expressed as

$$u = 2.07123\frac{\sin(\phi)}{\sin(\phi_{3dB})} \tag{4}$$

where ϕ_{3dB} is the constant 3-dB angle for the beam.

Next, the received signal at the desired destination node is given by

$$\begin{aligned} y_{R_{k*}D_m} &= G\vartheta_{d,m*}\sqrt{L_{D_m}P_R}\mathbf{h}^H_{R_{k*}D_m}\mathbf{w}_{R_{k*}D_m}y_{SR_{k*}} + n_{D_m} \\ &= G\mathbf{h}^H_{R_{k*}D_m}\mathbf{w}_{R_{k*}D_m}\sqrt{L_S L_{D_m} G_S(\phi) G_R P_S P_R} \\ &\quad \times \vartheta_{d,m*}\vartheta_{r,k*}\mathbf{h}_{SR_{k*}}\mathbf{w}^H_{SR_{k*}}\sum_{i=1}^{M}\varpi_i x_i \\ &\quad + G\vartheta_{d,m*}\sqrt{L_{D_m}P_R}\mathbf{h}^H_{R_{k*}D_m}\mathbf{w}_{R_{k*}D_m}\mathbf{n}_{R_{k*}} + n_{D_m} \end{aligned} \tag{5}$$

where $\mathbf{h}_{R_{k*}D_m} = [h_{R_{k*}D_m,1}, h_{R_{k*}D_m,2}, \ldots, h_{R_kD_m,N_T}]^T$ is the $N_T \times 1$ channel coefficient vector from R_{k*} to D_m, $\vartheta_{d,m*}$ denote the expected rain attenuation between R_{k*} and D_m, $\mathbf{w}_{R_kD_m} = \frac{\mathbf{h}_{R_kD_m}}{||\mathbf{h}_{R_kD_m}||_F}$ is the transmitting beamforming weight vector. Without loss of generality, the channel gains from R_k to D_m are ordered $h_{R_kD_1} \leqslant h_{R_kD_2} \leqslant \ldots h_{R_kD_M}$ and n_{D_m} is the zero mean additive white Gaussian noise (AWGN) with variance N_0. In the mmWave network, the path loss L_{D_m} in the terrestrial link can be modeled as [41]

$$L_{D_m} = \kappa + 10\nu\log(d_m) + \theta \tag{6}$$

where κ and ν denote the linear model parameters, θ is accounting for variances in shadowing fading and d_m denotes the distance between R_{k*} and D_m.

Following NOMA procedures [42], the received signal to interference and noise ratio (SINR) at m-th device to detect the information of q-th device ($m > q$) is given as follows (7), shown at the bottom of the next page. In which, $\bar{\eta}_m = L_S L_{D_m} G_S(\phi) G_R (\vartheta_{d,m*}\vartheta_{r,k*})^2$, $\eta = \frac{P_S}{N_0}$, $\eta_R = \frac{P_R}{N_0}$, $\rho_S = \eta_S \left\|\mathbf{h}_{SR_{k*}}\right\|_F^2$ and $\rho_{D_m} = \eta_R \left\|\mathbf{h}_{R_{k*}D_m}\right\|_F^2$.

Then the received SINR of m-th device to detect the information by treating $M-p$ devices's signals as interference is given by

$$\gamma_m = \frac{\rho_S\rho_{D_m}\bar{\eta}_m\varpi_m}{\bar{\eta}_m\rho_S\rho_{D_m}\sum\limits_{i=m+1}^{M}\varpi_i + \rho_{D_m}L_{D_m}\vartheta^2_{d,m*} + \rho_S\vartheta^2_{r,k} + 1} \tag{8}$$

After the information of $M-1$ devices can be detected, the received SINR for M-th device is given by

$$\gamma_M = \frac{\rho_S\rho_{D_M}\bar{\eta}_M\varpi_M}{\rho_{D_M}L_{D_M}\vartheta^2_{d,m*} + \rho_S\vartheta^2_{r,k} + 1} \tag{9}$$

III. STATISTICAL ANALYSIS

The rain attenuation is the important attenuation factor in mmWave band channels. The expected value of rain attenuation from S to R_{k*} link can be treated as a constant during a transmission phase. Hence, in order to reduce the computational complexity, satellite can select the desired relay node according to the feedback of expected rain attenuation rather than the channel gain vector, namely

$$k* = \arg\min_{k=1,\ldots,K}\left(\vartheta_{r,k}\right) \tag{10}$$

Therefore, the rain attenuation value of R_k can be expressed as $A* = \min(\vartheta_{r,1}, \ldots, \vartheta_{r,K})$. We then assume that the rain attenuation values are independently and identically distributed (IID). The cumulative density function (CDF) of $A*$ can be given by $F_{A*}(x) = 1-[1-F_A(x)]^K$, where $F_A(x)$ is the CDF of the lognormal rain attenuation distribution [43]. In order to investigate the effect of the different number of relays, we need to derive the expected value of $A*$, which can validate the means of our proposed relay selection scheme and shown in [6].

Next, we assume that the channel conditions of all hops are IID. Moreover, mmWave satellite-terrestrial communications are mainly impaired by the masking effect and weather conditions, especially rain attenuation [44]. Under the Shadowed-Rician fading model for the satellite links, the probability density function (PDF) of ρ_S is given by [45]

$$f_{\rho_S}(x) = \sum_{i_1=0}^{m_{SR}-1}\ldots\sum_{i_{N_R}=0}^{m_{SR}-1}\frac{\Xi(N_R)}{\eta_S^{\Lambda}}x^{\Lambda-1}e^{-\frac{\Delta}{\eta_S}x} \tag{11}$$

where

$$\Xi(N_R) = \prod_{\tau=1}^{N_R}\zeta(\xi_\tau)\alpha^{N_R}\prod_{\upsilon=1}^{N_R-1}\mathcal{B}\left(\sum_{l=1}^{\upsilon}\xi_l + \upsilon, \zeta_{\upsilon+1} + 1\right) \tag{12}$$

$\zeta(a) = \frac{(-1)^a(1-m_{SR})_a\delta^a}{(a!)^2}$, $\Lambda = \sum\limits_{\tau=1}^{N}\xi_\tau + N_R$, $\Delta = \beta_{SR} - \delta_{SR}$, $\alpha = \frac{\left(\frac{2b_{SR}m_{SR}}{2b_{SR}m_{SR}+\Omega_{SR}}\right)^{m_U}}{2b_{SR}}$, $\beta = \frac{1}{2b_{SR}}$ and $\delta = \frac{\Omega_{SR}}{2b_{SR}(2b_{SR}m_{SR}+\Omega_{SR})}$, Ω_{SR}, $2b_{SR}$ and m_SR are the average power of the LOS and multipath components and fading severity parameter, respectively. Based on [46, Eq. 3.351.2], the CDF of ρ_S is given as

$$F_{\rho_S}(x) = 1 - \sum_{i_1=0}^{m_{SR}-1}\ldots\sum_{i_{N_R}=0}^{m_{SR}-1}\Xi(N_R)\times\sum_{n=0}^{\Lambda-1}\frac{\Gamma(\Lambda)}{n!\Delta^{\Lambda-n}\eta_S^n}x^n e^{-\frac{\Delta}{\eta_S}x} \tag{13}$$

Considering the characterization of Nakagami-m fading, the PDF and CDF of unordered estimated channel gains $\tilde{\rho}_{D_m}$

are given respectively as [47]

$$f_{\tilde{\rho}_{D_m}}(x) = \left(\frac{\lambda_{RD_m}}{\eta_R}\right)^{m_{RD}N_T} \frac{x^{m_{RD}N_T-1} e^{-\frac{\lambda_{RD_m}x}{\eta_R}}}{\Gamma(m_{RD}N_T)} \tag{14}$$

$$F_{\tilde{\rho}_{D_m}}(x) = \frac{\gamma\left(m_{RD}N_T, \frac{\lambda_{RD_m}x}{\eta_R}\right)}{\Gamma(m_{RD}N_T)}, \tag{15}$$

where Ω_{RD_m} is the average power, $m_{RD} = m_{RD_1} = \ldots = m_{RD_M}$ is the fading severity and $\lambda_{RD_m} = \frac{m_{RD}}{\Omega_{RD_m}}$. Using order statistics [48], the PDF and CDF of the ordered channel gains ρ_{D_m} are respectively given by

$$f_{\rho_{D_m}}(x) = \Theta \sum_{a=0}^{M-m} (-1)^a \binom{M-m}{a} \times f_{\tilde{\rho}_{D_m}}(x) \left[F_{\tilde{\rho}_{D_m}}(x)\right]^{m+a-1} \tag{16}$$

$$F_{\rho_{D_m}}(x) = \Theta \sum_{a=0}^{M-m} \frac{(-1)^a}{m+a} \binom{M-m}{a} \left[F_{\tilde{\rho}_{D_m}}(x)\right]^{m+a} \tag{17}$$

where $\Theta = \frac{M!}{(m-1)!(M-m)!}$. Then, using the series form of $\gamma(\bullet,\bullet)$ in [46, Eq. 8.352.1] and applying binomial and multinomial expansions [46, 0.314], we can rewrite (16) as

$$\begin{aligned} f_{\rho_{D_m}}(x) &= \Theta \sum_{a=0}^{M-m} \sum_{b=0}^{m+a-1} \sum_{c=0}^{b(m_{RD}N_T-1)} \binom{M-m}{a} \\ &\times \binom{m+a-1}{b} \frac{(-1)^{a+b}\, \omega_c^b}{\Gamma(m_{RD}N_T)} \left(\frac{\lambda_{RD_m}}{\eta_R}\right)^{m_{RD}N_T+c} \\ &\times x^{m_{RD}N_T+c-1} e^{-\frac{\lambda_{RD}(b+1)}{\eta_R}x} \end{aligned} \tag{18}$$

where $\varepsilon_l = \frac{1}{l!}$, ω_c^b can be calculated as $\omega_0^b = \varepsilon_0^b$, $\omega_1^b = \varepsilon_1^b$, $\omega_{b(m_{RD}N_T-1)}^b = \varepsilon_{m_{RD}N_T-1}^b$, when $2 \leqslant c \leqslant m_{RD}N_T - 1$ we have $\omega_c^b = \frac{1}{c\varepsilon_0}\sum_{g=1}^{c}[gb-c+g]\varepsilon_g\omega_{c-g}^b$, and when $m_{RD}N_T \leqslant c \leqslant m_{RD}N_T - 1$, we have $\omega_c^b = \frac{1}{c\varepsilon_0}\sum_{g=1}^{m_{RD}N_T}[gb-c+g]\varepsilon_g\omega_{c-g}^b$.

IV. PERFORMANCE ANALYSIS

In this section, the outage performance of the satellite network cooperative with NOMA will be analyzed in terms of outage probability and system diversity order. To this end, both exact and asymptotic expressions for the outage probability will be studied.

A. OUTAGE PROBABILITY

The outage event will occur at D_m if D_m fails to decode its own signal or the signal of D_q. The outage probability at D_m is expressed as

$$P_m = 1 - \Pr\left\{\mathrm{E}_{m,1}, \mathrm{E}_{m,2}, \ldots, \mathrm{E}_{m,m}\right\} \tag{19}$$

where $\mathrm{E}_{m,q}$ denotes the event that D_m can successfully detect the D_q's signal and can be given by

$$E_{m,q} = \left\{\gamma_{m\to q} > \gamma_{th_q}\right\} \tag{20}$$

where γ_{th_q} denotes the target rate of D_q.

Proposition 1: The closed-form outage probability of device D_m can be expressed as (21), shown at the bottom of the next page.

Proof: Substituting (7) into (20) and putting the result into (19), we can write P_m as (22), shown at the bottom of the next page.

where $\vartheta_m = \frac{\gamma_{th_m}}{\bar{\eta}_m\left(\varpi_m - \gamma_{th_m}\sum_{i=m+1}^{M}\varpi_i\right)}$, $\varpi_m > \gamma_{th_m}\sum_{i=m+1}^{M}\varpi_i$, $\vartheta_m^* = \max(\vartheta_1, \vartheta_2, \ldots, \vartheta_m)$. Then, putting (13) and (18) into (22), we claim

$$\begin{aligned} P_m &= 1 - \Theta \sum_{i_1=0}^{m_{SR}-1} \cdots \sum_{i_{N_R}=0}^{m_{SR}-1} \frac{\Gamma(\Lambda)\,\Xi(N_R)}{n!\Delta^{\Lambda-n}\eta_S^n} \sum_{a=0}^{M-m}\sum_{b=0}^{m+a-1} \\ &\times \sum_{c=0}^{b(m_{RD}N_T-1)} \binom{M-m}{a}\binom{m+a-1}{b} \frac{(-1)^{a+b}\,\omega_c^b}{\Gamma(m_{RD}N_T)} \\ &\times \int_{\vartheta_m^*\vartheta_{r,k*}^2}^{\infty} \left(\frac{\lambda_{RD_m}}{\eta_R}\right)^{m_{RD}N_T+c} x^{m_{RD}N_T+c-1} e^{-\frac{\lambda_{RD}(b+1)}{\eta_R}x} \\ &\times \left(\frac{\vartheta_m^*\left(xL_{D_m}\vartheta_{d,m*}^2+1\right)}{x-\vartheta_m^*\vartheta_{r,k*}^2}\right)^n e^{-\frac{\vartheta_m^*\Delta\left(xL_{D_m}\vartheta_{d,m*}^2+1\right)}{\eta_S\left(x-\vartheta_m^*\vartheta_{r,k*}^2\right)}}\, dx \end{aligned} \tag{23}$$

Put $t = x - \vartheta_m^*\vartheta_{r,k*}^2 \Rightarrow x = t + \vartheta_m^*\vartheta_{r,k*}^2$, (23) can be calculated as follows

$$\begin{aligned} P_m &= 1 - \Theta \sum_{i_1=0}^{m_{SR}-1} \cdots \sum_{i_{N_R}=0}^{m_{SR}-1} \frac{\Gamma(\Lambda)\,\Xi(N_R)}{n!\Delta^{\Lambda-n}} \sum_{a=0}^{M-m}\sum_{b=0}^{m+a-1} \\ &\times \sum_{c=0}^{b(m_{RD}N_T-1)} \binom{M-m}{a}\binom{m+a-1}{b} \frac{(-1)^{a+b}\,\omega_c^b}{\Gamma(m_{RD}N_T)} \end{aligned}$$

$$\begin{aligned} \gamma_{m\to q} &= \frac{\bar{\eta}_m P_S P_R G^2 \left\|\mathbf{h}_{SR_{k*}}\right\|_F^2 \left\|\mathbf{h}_{R_{k*}D_m}\right\|_F^2 \varpi_q}{\bar{\eta}_m P_S P_R G^2 \left\|\mathbf{h}_{SR_{k*}}\right\|_F^2 \left\|\mathbf{h}_{R_{k*}D_m}\right\|_F^2 \sum_{i=q+1}^{M}\varpi_i + \left(G\vartheta_{d,m*}\right)^2 P_R L_{D_m} \left\|\mathbf{h}_{R_{k*}D_m}\right\|_F^2 N_0 + N_0} \\ &= \frac{\rho_S\rho_{D_m}\bar{\eta}_m\varpi_q}{\bar{\eta}_m\rho_S\rho_{D_m}\sum_{i=q+1}^{M}\varpi_i + \rho_{D_m}L_{D_m}\vartheta_{d,m*}^2 + \rho_S\vartheta_{r,k*}^2 + 1} \end{aligned} \tag{7}$$

$$\times \left(\frac{\lambda_{RD_m}}{\eta_R}\right)^{m_{RD}N_T+c} \left(\frac{\vartheta_m^*}{\eta_S}\right)^n e^{-\Phi_2\vartheta_m^*}$$
$$\times \int_0^\infty \left(t+\vartheta_m^*\vartheta_{r,k*}^2\right)^{m_{RD}N_T+c-1} e^{-\Phi_1 t} e^{-\frac{\vartheta_m^*\Delta(\Phi_3\vartheta_m^*+1)}{\eta_S t}}$$
$$\times \left(\frac{tL_{D_m}\vartheta_{d,m*}^2+\vartheta_m^* L_{D_m}\vartheta_{d,m*}^2\vartheta_{r,k*}^2+1}{t}\right)^n dt \quad (24)$$

where $\Phi_1 = \frac{\lambda_{RD}(b+1)}{\eta_R}$, $\Phi_2 = \frac{\lambda_{RD}\vartheta_{r,k*}^2(b+1)}{\eta_R} + \frac{\Delta L_{D_m}\vartheta_{d,m*}^2}{\eta_S}$, $\Phi_3 = L_{D_m}\vartheta_{d,m*}^2\vartheta_{r,k*}^2$. Next using [46, Eq 1.111], we can rewrite (24) as

$$P_m = 1 - \Theta \sum_{i_1=0}^{m_{SR}-1} \cdots \sum_{i_{N_R}=0}^{m_{SR}-1} \sum_{n=0}^{\Lambda-1} \sum (a,b,c,d,e)$$
$$\times \frac{\Xi(N_R)\Gamma(\Lambda)(-1)^{a+b}\omega_c^b e^{-\Phi_2\vartheta_m^*}\left(\Phi_3\vartheta_m^*\right)^d}{n!\Delta^{\Lambda-n}\Gamma(m_{RD}N_T)\left(\vartheta_m^*\vartheta_{r,k*}^2\right)^{-(m_{RD}N_T+c-e-1)}}$$
$$\times \left(\frac{\vartheta_m^*}{\eta_S}\right)^n \times \left(\frac{\lambda_{RD_m}}{\eta_R}\right)^{m_{RD}N_T+c} \int_0^\infty t^{e-n} e^{-\Phi_1 t}$$
$$\times e^{-\frac{\vartheta_m^*\Delta(\Phi_3\vartheta_m^*+1)}{\eta_S t}} dt \quad (25)$$

where

$$\sum(a,b,c,d,e) = \sum_{a=0}^{M-m}\sum_{b=0}^{m+a-1}\sum_{c=0}^{b(m_{RD}N_T-1)}\sum_{d=0}^{n}\sum_{e=0}^{m_{RD}N_T+c+d-1}$$
$$\times \binom{M-m}{a}\binom{m+a-1}{b}\binom{n}{d}\binom{m_{RD}N_T+c+d-1}{e} \quad (26)$$

Based on [46, Eq. 3.471.9], the integral in (25) can be calculated. And the proof is complete.

B. DIVERSITY ORDER

For more insights, the order of diversity is analyzed. For this, in the high SNR regime, we assume $\eta = \eta_S = \eta_R \to \infty$. Then, the diversity order of the terrestrial device can be given by [24] and [49]

TABLE 3. Channel parameters [23], [29], [34].

Shadowing	Frequent heavy shadowing (FHS)	Average shadowing (AS)
b_{SR}	0.063	0.251
m_{SR}	1	5
Ω_{SR}	0.0007	0.279

$$D = -\lim_{\eta\to\infty}\frac{\log\left(P_m^\infty(\eta)\right)}{\log(\eta)} \quad (27)$$

where $P_m^\infty(\eta)$ denotes the asymptotic outage probability.

Proposition 2: The asymptotic outage probability of the device D_m in the high SNR regime is given by

$$P_m^\infty \approx \frac{\alpha^{N_R}}{(N_R)!\eta_S^{N_R}}\left(\frac{\bar{\vartheta}_m^*}{\vartheta_{r,k*}^2}\right)^{N_R} + \left(\frac{\lambda_{RD_m}}{\eta_R}\right)^{m_{RD}N_T m}$$
$$\times \frac{\Theta}{m\left[\Gamma(m_{RD}N_T+1)\right]^m}\left(\frac{\bar{\vartheta}_m^*}{L_{D_m}\vartheta_{d,m*}^2}\right)^{m_{RD}N_T m} \quad (28)$$

Proof: See Appendix A

Remark: Upon substituting (28) into (27), the achievable diversity order of m-th device is $\min(N_R, m_{RD}N_T m)$

C. ERGODIC CAPACITY (EC)

In this section, the ergodic rate of m-th device is discussed in detail, where the target rates of devices are determined by the channel conditions. Next, m-th device detects the q-th device's information successfully, since it holds $h_{R_kD_m} \geqslant h_{R_kD_p}$. In this situation, the achievable rate of m-th is expressed as $\tilde{R}_m = \frac{1}{2}\log_2(1+\gamma_m)$. Thus, the ergodic rates of m-th and M-th device are as follows

$$\tilde{R}_{m,ave} = \mathbb{E}\left\{\frac{1}{2}\log_2(1+\gamma_m)\right\} \quad (29)$$

and

$$\tilde{R}_{M,ave} = \mathbb{E}\left\{\frac{1}{2}\log_2(1+\gamma_M)\right\} \quad (30)$$

$$P_m = 1 - 2\Theta \sum_{i_1=0}^{m_{SR}-1} \cdots \sum_{i_{N_R}=0}^{m_{SR}-1} \sum_{n=0}^{\Lambda-1} \sum (a,b,c,d,e) \frac{\Xi(N_R)\Gamma(\Lambda)(-1)^{a+b}\omega_c^b\left(\Phi_3\vartheta_m^*\right)^d e^{-\Phi_2\vartheta_m^*}}{n!\Delta^{\Lambda-n}\Gamma(m_{RD}N_T)\left(\vartheta_m^*\vartheta_{r,k*}^2\right)^{-(m_{RD}N_T+c-e-1)}}$$
$$\times \left(\frac{\lambda_{RD_m}}{\eta_R}\right)^{m_{RD}N_T+c}\left(\frac{\vartheta_m^*}{\eta_S}\right)^n\left(\frac{\vartheta_m^*\Delta\left(\Phi_3\vartheta_m^*+1\right)}{\eta_S\Phi_1}\right)^{\frac{e-n+1}{2}} K_{e-n+1}\left(2\sqrt{\frac{\Delta\Phi_1\vartheta_m^*\left(\Phi_3\vartheta_m^*+1\right)}{\eta_S}}\right) \quad (21)$$

$$P_m = 1 - \Pr\left(\rho_S > \frac{\vartheta_m^*\left(\rho_{D_m}L_{D_m}\vartheta_{d,m*}^2+1\right)}{\rho_{D_m}-\vartheta_m^*\vartheta_{r,k*}^2}, \rho_{D_m} > \vartheta_m^*\vartheta_{r,k*}^2\right) = 1 - \int_{\vartheta_m^*\vartheta_{r,k*}^2}^\infty f_{\rho_{D_m}}(x)\left\{1 - F_{\rho_S}\left(\frac{\vartheta_m^*\left(xL_{D_m}\vartheta_{d,m*}^2+1\right)}{x-\vartheta_m^*\vartheta_{r,k*}^2}\right)\right\} dx \quad (22)$$

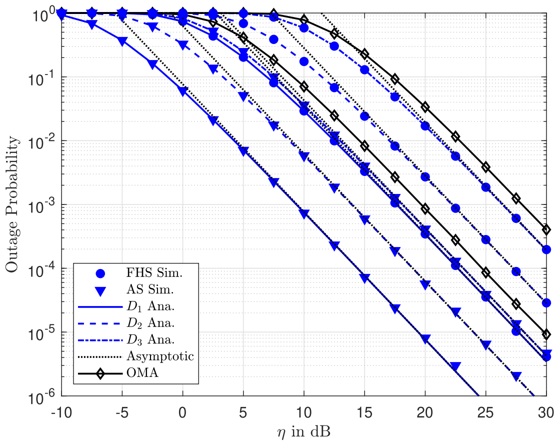

FIGURE 2. The outage probability of D_m versus transmit η in dB varying the parameter of satellite links with $K = 1$.

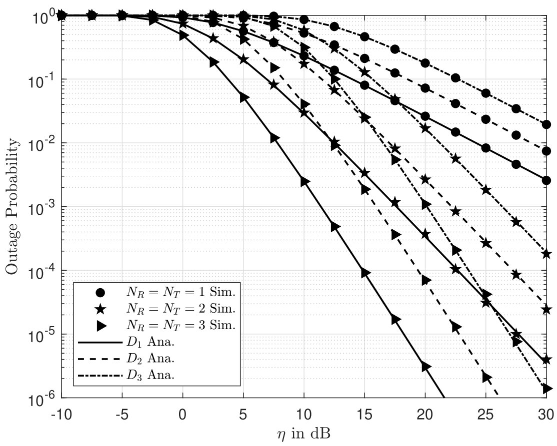

FIGURE 3. The outage probability of D_m versus transmit η in dB varying the transmit and received antenna of R_{k*} with $K = 1$ and the satellite link in FHS case.

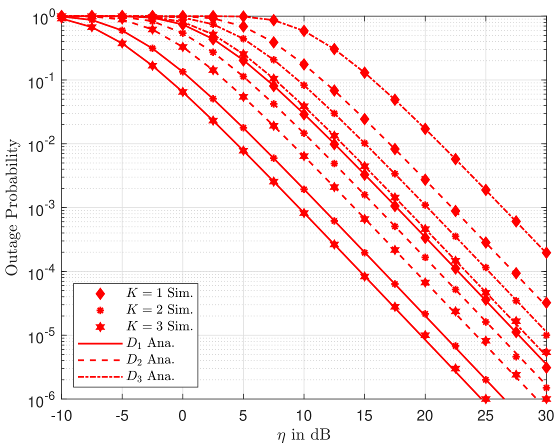

FIGURE 4. The outage probability of D_m versus transmit η in dB varying the number of Relay with the satellite link in FHS case.

Proposition 3: The closed-form of ergodic rate for m-th and M-th device are given by (31) and (32), respectively, as shown at the bottom of the next page.

Proof: See Appendix B

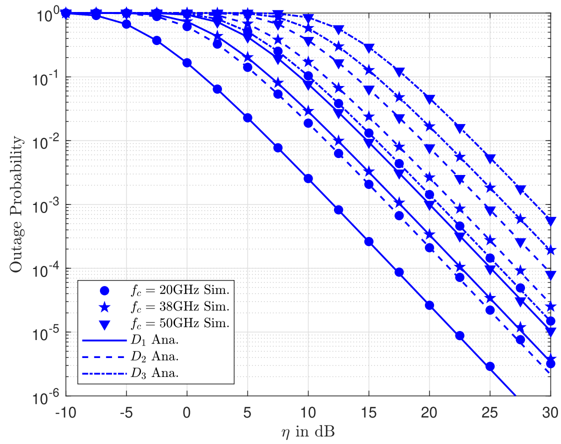

FIGURE 5. The outage probability versus transmit η in dB varying the carrier frequency in FHS case.

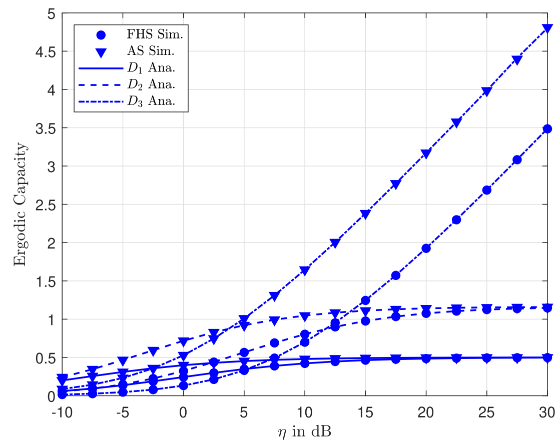

FIGURE 6. The Ergodic Capacity of D_m versus transmit η in dB varying the parameter of satellite links with $N_R = N_T = K = 1$.

V. NUMERICAL RESULTS

In this section, to verify the mathematical analysis, it is necessary to simulate and illustrate the proposed assisted NOMA scheme. Here, the shadowing scenarios of the satellite links, including frequent heavy shadowing (FHS) and average shadowing (AS) being given in Table 3. Furthermore, the parameters can be provided in Table 4. Monte Carlo simulations are performed to validate the analytical results shown in the following figures.

In Figure 2, we show the OP versus η in dB with different satellite links. First, the performance of the devices will be improved by increasing the transmit power. Next, the performance of device D_1 is the best due to the power allocation of D_1 is better than D_2 and D_3. Moreover, the improvement of satellite link also greatly improves device performance, i.e. AS is the best case. Furthermore, the system uses the NOMA scheme that is better than OMA. The fundamental cause is that OMA-based systems require more time slots than NOMA-based systems to process the same number of devices. Over the whole SNR range, Monte Carlo simulation curves and analytical results accord very well. At high SNR, it can be seen that the asymptotic OP curves closely reflect the actual findings.

TABLE 4. Simulation parameter [50], [51], [52].

Parameter	Value
The number of device	$M = 3$
The number of Relay	$K = 2$
The number of received antenna at relays	$N_R = 2$
The number of transmit antenna at relays	$N_T = 2$
Satellite Orbit	GEO
Frequency band	38 GHz
Bandwidth	500 MHz
Noise temperature	300 K
Maximal beam gain	48 dBi
Antenna gain at R_{k*}	4 dBi
Angle between the satellite and relay	0.3^o
Angle ϕ_{3dB}	0.4^o
Path loss exponents	$\kappa = 118.77$, $\nu = 5.78$ and $\theta = 0.12$
Distance between R_{k*} and devices	$d_1 = 0.5$km, $d_2 = 0.4$km and $d_3 = 0.3$km
The power allocation	$\varpi_1 = 0.5$, $\varpi_2 = 0.4$ and $\varpi_1 = 0.1$
The target rate	$R_1 = 0.4$, $R_2 = 0.9$ and $R_3 = 1.2$
The fading severity	$m_{RD} = m_{RD_1} = m_{RD_2} = m_{RD_3} = 1$
The average power	$\Omega_{RD_1} = \Omega_{RD_2} = \Omega_{RD_3} = 1$
The expected rain attenuation	$\vartheta_{d_m} = 0.5$dB

Figure 3 shows the OP versus η in dB under the influence of the relay antenna. We can easily see that increasing the number of antennas at the relay will significantly improve the system's performance. It proves the superiority of installing multiple antennas in the system. Compared to the case of the relay with $N_R = N_T = 2$, the large OP gap can be seen once the relay is designed with $N_R = N_T = 3$. The explanation is that a design with more diversity from many antennas could enhance the signal received for the devices on the ground. Figure 4 shows the simulation OP versus η in dB with different numbers of relays. When the number of relays is increased, the performance is improved more. It demonstrates the effectiveness of using a relay selection scheme.

Fig. 5 shows The OP versus transmit η in dB varying the carrier frequency. It can be observed that the higher the carrier frequency the worse the OP. The rationale behind this phenomenon is that with higher frequency, the path-loss

$$\tilde{R}_{m,ave} \approx \frac{\Theta\pi\varpi_m}{2\ln(2)I}\sum_{i_1=0}^{m_{SR}-1}\cdots\sum_{i_{N_R}=0}^{m_{SR}-1}\sum_{n=0}^{\Lambda-1}\sum(a,b,c,d,e)\sum_{k=1}^{I}\sqrt{1-\varphi_k^2}\,\frac{\Xi(N_R)\Gamma(\Lambda)(-1)^{a+b}\omega_c^b\left(\lambda_{RD_m}/\eta_R\right)^{m_{RD}N_T+c}(\Phi_3)^d}{n!\Delta^{\Lambda-n}\Gamma(m_{RD}N_T)\left(\vartheta_{r,k*}^2\right)^{-(m_{RD}N_T+c-e-1)}\eta_S^n}$$
$$\times\frac{e^{-\Phi_2\hat{\vartheta}_m\left(\frac{(\varphi_k+1)\varpi_m}{\tilde{\varpi}_m}\right)}}{(\tilde{\varpi}_m+(\varphi_k+1)\varpi_m)}\left(\frac{\Delta\left(\Phi_3\hat{\vartheta}_m\left(\frac{(\varphi_k+1)\varpi_m}{\tilde{\varpi}_m}\right)+1\right)}{\eta_S\Phi_1}\right)^{\frac{e-n+1}{2}}\left(\hat{\vartheta}_m\left(\frac{(\varphi_k+1)\varpi_m}{\tilde{\varpi}_m}\right)\right)^{\frac{2(m_{RD}N_T+d+c)+n-e-1}{2}}$$
$$\times K_{e-n+1}\left(2\sqrt{\frac{\Delta\Phi_1\hat{\vartheta}_m\left(\frac{(\varphi_k+1)\varpi_m}{\tilde{\varpi}_m}\right)\left(\Phi_3\hat{\vartheta}_m\left(\frac{(\varphi_k+1)\varpi_m}{\tilde{\varpi}_m}\right)+1\right)}{\eta_S}}\right) \quad (31)$$

$$\tilde{R}_{M,ave} \approx \frac{\pi^2\Theta}{4I\ln(2)}\sum_{i_1=0}^{m_{SR}-1}\cdots\sum_{i_{N_R}=0}^{m_{SR}-1}\sum_{n=0}^{\Lambda-1}\sum(a,b,c,d,e)\sum_{k=1}^{I}\sqrt{1-\varphi_k^2}\sec^2\left((\varphi_k+1)\frac{\pi}{4}\right)$$
$$\times\frac{\Xi(N_R)\Gamma(\Lambda)(-1)^{a+b}\omega_c^b(\Phi_3)^d}{n!\Delta^{\Lambda-n}\eta_S^n\Gamma(m_{RD}N_T)\left(\vartheta_{r,k*}^2\right)^{-(m_{RD}N_T+c-e-1)}}$$
$$\times\frac{e^{-\Phi_2\hat{\vartheta}_M\left(\tan\left(\frac{(\varphi_k+1)\pi}{4}\right)\right)}}{\left(1+\tan\left(\frac{(\varphi_k+1)\pi}{4}\right)\right)}\left(\hat{\vartheta}_M\left(\tan\left(\frac{(\varphi_k+1)\pi}{4}\right)\right)\right)^{\frac{2(m_{RD}N_T+c+d)+n-e-1}{2}}\left(\frac{\Delta\left(\Phi_3\hat{\vartheta}_M\left(\tan\left(\frac{(\varphi_k+1)\pi}{4}\right)\right)+1\right)}{\eta_S\Phi_1}\right)^{\frac{e-n+1}{2}}$$
$$\times\left(\frac{\lambda_{RD_m}}{\eta_R}\right)^{m_{RD}N_T+c}K_{e-n+1}\left(2\sqrt{\frac{\Delta\Phi_1\hat{\vartheta}_M\left(\tan\left(\frac{(\varphi_k+1)\pi}{4}\right)\right)\left(\Phi_3\hat{\vartheta}_M\left(\tan\left(\frac{(\varphi_k+1)\pi}{4}\right)\right)+1\right)}{\eta_S}}\right) \quad (32)$$

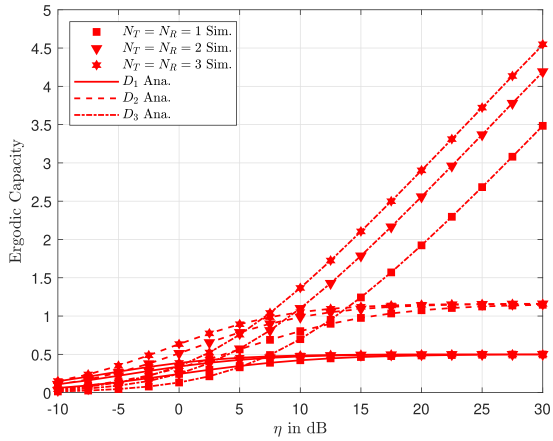

FIGURE 7. The Ergodic Capacity of D_m versus transmit η in dB varying the transmit and received antenna of R_{k*} with $K = 1$ and the satellite link in FHS case.

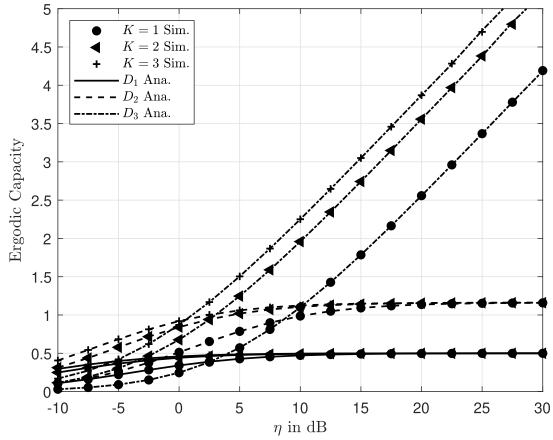

FIGURE 8. The Ergodic Capacity of D_m versus transmit η in dB varying the number of Relay with the satellite link in FHS case.

drops dramatically thus an appropriate antenna beamforming gain is necessary to compensate such losses. Regarding the selection of the 38GHz, we choose because it is in the range of GEO operation [41], [50].

Figure 6 indicates the EC versus η with different satellite links, as well as Figure 2. The EC rates at D_1 and D_2 are almost no change for the FHS and AS case. But the difference between the EC curves at D_3 in both modes is comparably quite large. Moreover, when increasing in high SNR, the gap of D_3 is different with D_2 and D_1.

Figure 7 and Figure 8 show the EC of D_m versus η in dB varying the number of relay antennas and the number of relays, respectively. For EC of D_1 and D_2, the gaps between cases change only in the low SNR region and will intersect at a point in the high region. Therefore, changing the number of antennas and the number of relays does not have much effect on EC. But for the EC of D_3, the gaps between instances will be large. It shows the effect of the number of antennas and the number of relays to the EC.

VI. CONCLUSION

In this article, we investigated the performance of NOMA-based HSTRN with mmWave network where the devices are supported by multiple relays. Unlike previous studies, we consider multiple antennas receiving and transmitting at relay and NOMA in the context of serving multiple devices. In addition, we use the rain attenuation value to choose the best relay. The closed-form of OP, EC, and asymptotic expressions of OP were developed based on the model of the considered system. To support those performance studies and demonstrate how important factors like fading and rain attenuation affect system performance, simulations have been made available. Our results showed that the OP of the system under consideration can be greatly improved compared to the OMA scheme, highlighting the advantages of implementing the NOMA scheme to the system. These results provide a theoretical framework for further investigation.

APPENDIX A

First, when $\eta_S \rightarrow \infty$ and apply the Maclaurin series expansion of the exponential function in (11). So, the PDF of ρ_S can be approximated as

$$f_{\rho_S}(x) = \frac{\alpha^{N_R} x^{N_R} - 1}{(N_R - 1)! \eta_S^{N_R}} \tag{33}$$

Next, the CDF ρ_S has asymptotic behavior as

$$F_{\rho_S}(x) = \frac{\alpha^{N_R} x^{N_R}}{(N_R)! \eta_S^{N_R}} \tag{34}$$

Furthermore, when $\eta_R \rightarrow \infty$ and taking the first term ($a = 0$ of series representation, the asymptotic behavior of CDF ρ_{D_m} can be obtained as

$$F_{\rho_{D_m}}(x) = \frac{\Theta}{m\left[\Gamma\left(m_{RD} N_T + 1\right)\right]^m} \times \left(\frac{\lambda_{RD_m}}{\eta_R}\right)^{m_{RD} N_T m} x^{m_{RD} N_T m} \tag{35}$$

Then, the asymptotic P_m^{∞} can be expressed as

$$P_m^{\infty} \approx 1 - \Pr\left(\frac{\rho_{D_m} L_{D_m} \vartheta_{d,m*}^2 \rho_S \vartheta_{r,k*}^2}{\rho_{D_m} L_{D_m} \vartheta_{d,m*}^2 + \rho_S \vartheta_{r,k*}^2} > \bar{\vartheta}_m^*\right) \tag{36}$$

Using the inequality $\frac{uv}{u+v} \leqslant \min(u, v)$. Thus, the asymptotic P_m^{∞} can be calculated as

$$\begin{aligned} P_m^{\infty} &\approx 1 - \Pr\left(\min\left(\rho_{D_m} L_{D_m} \vartheta_{d,m*}^2, \rho_S \vartheta_{r,k*}^2\right) > \bar{\vartheta}_m^*\right) \\ &\approx F_{D_m}^{\infty}\left(\frac{\bar{\vartheta}_m^*}{L_{D_m} \vartheta_{d,m*}^2}\right) + F_{\rho_S}^{\infty}\left(\frac{\bar{\vartheta}_m^*}{\vartheta_{r,k*}^2}\right) \\ &\quad - F_{\rho_S}^{\infty}\left(\frac{\bar{\vartheta}_m^*}{\vartheta_{r,k*}^2}\right) F_{D_m}^{\infty}\left(\frac{\bar{\vartheta}_m^*}{L_{D_m} \vartheta_{d,m*}^2}\right) \end{aligned} \tag{37}$$

With help (34) and (35), we can obtain as

$$\begin{aligned} P_m^{\infty} &\approx \frac{\alpha^{N_R}}{(N_R)! \eta_S^{N_R}} \left(\frac{\bar{\vartheta}_m^*}{\vartheta_{r,k*}^2}\right)^{N_R} + \left(\frac{\lambda_{RD_m}}{\eta_R}\right)^{m_{RD} N_T m} \\ &\quad \times \frac{\Theta}{m\left[\Gamma\left(m_{RD} N_T + 1\right)\right]^m} \left(\frac{\bar{\vartheta}_m^*}{L_{D_m} \vartheta_{d,m*}^2}\right)^{m_{RD} N_T m} \end{aligned} \tag{38}$$

APPENDIX B

The ergodic rate of m-th device can be calculated as

$$\tilde{R}_{m,ave} = \frac{1}{2\ln(2)} \int_0^{\frac{\varpi_m}{\tilde{\varpi}_m}} \frac{1 - F_{\gamma_m}(x)}{1+x} dx \tag{39}$$

where $\tilde{\varpi}_m = \sum_{i=m+1}^{M} \varpi_i$. Similarly, Proposition 1, the CDF of γ_m can be obtained as

$$\begin{aligned} &F_{\gamma_m}(x) \\ &= 1 - 2\Theta \sum_{i_1=0}^{m_{SR}-1} \cdots \sum_{i_{N_R}=0}^{m_{SR}-1} \sum_{n=0}^{\Lambda-1} \sum (a,b,c,d,e) \\ &\times \frac{\Xi(N_R)\Gamma(\Lambda)(-1)^{a+b}\omega_c^b \left(\Phi_3\hat{\vartheta}_m(x)\right)^d e^{-\Phi_2\hat{\vartheta}_m(x)}}{n!\Delta^{\Lambda-n}\Gamma(m_{RD}N_T)\left(\hat{\vartheta}_m(x)\vartheta_{r,k*}^2\right)^{-(m_{RD}N_T+c-e-1)}} \\ &\times \left(\frac{\lambda_{RD_m}}{\eta_R}\right)^{m_{RD}N_T+c} \left(\frac{\hat{\vartheta}_m(x)\Delta\left(\Phi_3\hat{\vartheta}_m(x)+1\right)}{\eta_S\Phi_1}\right)^{\frac{e-n+1}{2}} \\ &\times \left(\frac{\hat{\vartheta}_m(x)}{\eta_S}\right)^n K_{e-n+1}\left(2\sqrt{\frac{\Delta\Phi_1\hat{\vartheta}_m(x)\left(\Phi_3\hat{\vartheta}_m(x)+1\right)}{\eta_S}}\right) \end{aligned} \tag{40}$$

where $\hat{\vartheta}_m(x) = \frac{x}{\bar{\eta}_m(\varpi_m - x\tilde{\varpi}_m)}$. Putting (34) into (33), we can calculate $\tilde{R}_{m,ave}$ as

$$\begin{aligned} \tilde{R}_{m,ave} &= \frac{\Theta}{\ln(2)} \sum_{i_1=0}^{m_{SR}-1} \cdots \sum_{i_{N_R}=0}^{m_{SR}-1} \sum_{n=0}^{\Lambda-1} \sum (a,b,c,d,e) \\ &\times \frac{\Xi(N_R)\Gamma(\Lambda)(-1)^{a+b}\omega_c^b\left(\lambda_{RD_m}/\eta_R\right)^{m_{RD}N_T+c}}{n!\Delta^{\Lambda-n}\Gamma(m_{RD}N_T)\left(\vartheta_{r,k*}^2\right)^{-(m_{RD}N_T+c-e-1)}} \\ &\times \int_0^{\frac{\varpi_m}{\tilde{\varpi}_m}} \frac{\left(\Phi_3\hat{\vartheta}_m(x)\right)^d e^{-\Phi_2\hat{\vartheta}_m(x)}}{(1+x)\left(\hat{\vartheta}_m(x)\right)^{-(m_{RD}N_T+c-e-1)}} \\ &\times \left(\frac{\hat{\vartheta}_m(x)\Delta\left(\Phi_3\hat{\vartheta}_m(x)+1\right)}{\eta_S\Phi_1}\right)^{\frac{e-n+1}{2}} \left(\frac{\hat{\vartheta}_m(x)}{\eta_S}\right)^n \\ &\times K_{e-n+1}\left(2\sqrt{\frac{\Delta\Phi_1\hat{\vartheta}_m(x)\left(\Phi_3\hat{\vartheta}_m(x)+1\right)}{\eta_S}}\right) dx \end{aligned} \tag{41}$$

Using the Gauss-Chebyshev quadrature [53] into the equation (41) with $\varphi_k = \cos\left(\frac{2k-1}{2I}\pi\right)$, we obtain (31).

Next, the ergodic rate of M-th device can be calculated as

$$\tilde{R}_{M,ave} = \frac{1}{2\ln(2)} \int_0^{\infty} \frac{1 - F_{\gamma_M}(x)}{1+x} dx \tag{42}$$

Similarly, the PDF of γ_M can be expressed as

$$\begin{aligned} &F_{\gamma_M}(x) \\ &= 1 - 2\Theta \sum_{i_1=0}^{m_{SR}-1} \cdots \sum_{i_{N_R}=0}^{m_{SR}-1} \sum_{n=0}^{\Lambda-1} \sum (a,b,c,d,e) \\ &\times \frac{\Xi(N_R)\Gamma(\Lambda)(-1)^{a+b}\omega_c^b\left(\Phi_3\hat{\vartheta}_M(x)\right)^d e^{-\Phi_2\hat{\vartheta}_M(x)}}{n!\Delta^{\Lambda-n}\Gamma(m_{RD}N_T)\left(\hat{\vartheta}_M(x)\vartheta_{r,k*}^2\right)^{-(m_{RD}N_T+c-e-1)}} \\ &\times \left(\frac{\lambda_{RD_m}}{\eta_R}\right)^{m_{RD}N_T+c} \left(\frac{\hat{\vartheta}_M(x)\Delta\left(\Phi_3\hat{\vartheta}_m(x)+1\right)}{\eta_S\Phi_1}\right)^{\frac{e-n+1}{2}} \\ &\times \left(\frac{\hat{\vartheta}_M(x)}{\eta_S}\right)^n K_{e-n+1}\left(2\sqrt{\frac{\Delta\Phi_1\hat{\vartheta}_M(x)\left(\Phi_3\hat{\vartheta}_M(x)+1\right)}{\eta_S}}\right) \end{aligned} \tag{43}$$

where $\hat{\vartheta}_M(x) = \frac{x}{\bar{\eta}_m\varpi_M}$. Putting (43) into (42), the ergodic rate of M-th device can be calculated as

$$\begin{aligned} &\tilde{R}_{M,ave} \\ &= \frac{\Theta}{\ln(2)} \sum_{i_1=0}^{m_{SR}-1} \cdots \sum_{i_{N_R}=0}^{m_{SR}-1} \sum_{n=0}^{\Lambda-1} \sum (a,b,c,d,e) \\ &\times \frac{\Xi(N_R)\Gamma(\Lambda)(-1)^{a+b}\omega_c^b\left(\lambda_{RD_m}/\eta_R\right)^{m_{RD}N_T+c}}{n!\Delta^{\Lambda-n}\Gamma(m_{RD}N_T)\left(\vartheta_{r,k*}^2\right)^{-(m_{RD}N_T+c-e-1)}} \\ &\times \int_0^{\infty} \frac{\left(\Phi_3\hat{\vartheta}_M(x)\right)^d e^{-\Phi_2\hat{\vartheta}_M(x)}}{(1+x)\left(\hat{\vartheta}_M(x)\right)^{-(m_{RD}N_T+c-e-1)}} \\ &\times \left(\frac{\hat{\vartheta}_M(x)\Delta\left(\Phi_3\hat{\vartheta}_M(x)+1\right)}{\eta_S\Phi_1}\right)^{\frac{e-n+1}{2}} \left(\frac{\hat{\vartheta}_M(x)}{\eta_S}\right)^n \\ &\times K_{e-n+1}\left(2\sqrt{\frac{\Delta\Phi_1\hat{\vartheta}_M(x)\left(\Phi_3\hat{\vartheta}_M(x)+1\right)}{\eta_S}}\right) dx \end{aligned} \tag{44}$$

Furthermore, we set $t = \frac{4\arctan(x)}{\pi} - 1 \Rightarrow x = \tan\left(\frac{(t+1)\pi}{4}\right)$, $dx = \frac{\pi}{4}\sec^2\left(\frac{(t+1)\pi}{4}\right)$ and using the Gaussian-Chebyshev quadrature. We can approximate the ergodic rate $\tilde{R}_{M,ave}$ as (32).

The proof is complete.

REFERENCES

[1] D. Tse and P. Viswanath, *Fundamentals of Wireless Communication*. Cambridge, U.K.: Digital Library Digital Library, 2005.

[2] K. Y. Jo, *Satellite Communications Network Design and Analysis*. Norwood, MA, USA: Artech House, 2011.

[3] Q. Huang, M. Lin, W.-P. Zhu, J. Cheng, and M.-S. Alouini, ''Uplink massive access in mixed RF/FSO satellite-aerial-terrestrial networks,'' *IEEE Trans. Commun.*, vol. 69, no. 4, pp. 2413–2426, Apr. 2021.

[4] K. Guo, ''Physical layer security for multiuser satellite communication systems with threshold-based scheduling scheme,'' *IEEE Trans. Veh. Technol.*, vol. 69, no. 5, pp. 5129–5141, May 2020.

[5] Z. Lin, M. Lin, B. Champagne, W.-P. Zhu, and N. Al-Dhahir, ''Secure and energy efficient transmission for RSMA-based cognitive satellite-terrestrial networks,'' *IEEE Wireless Commun. Lett.*, vol. 10, no. 2, pp. 251–255, Feb. 2021.

[6] X. Liang, J. Jiao, S. Wu, and Q. Zhang, ''Outage analysis of multirelay multiuser hybrid satellite-terrestrial millimeter-wave networks,'' *IEEE Wireless Commun. Lett.*, vol. 7, no. 6, pp. 1046–1049, Dec. 2018.

[7] S. Gu, J. Jiao, Z. Huang, S. Wu, and Q. Zhang, ''ARMA-based adaptive coding transmission over millimeter-wave channel for integrated satellite-terrestrial networks,'' *IEEE Access*, vol. 6, pp. 21635–21645, 2018.

[8] X. Liang, J. Jiao, B. Feng, S. Wu, B. Cao, and Q. Zhang, ''Performance analysis of millimeter-wave hybrid satellite-terrestrial relay networks over rain fading channel,'' in *Proc. IEEE 88th Veh. Technol. Conf. (VTC-Fall)*, Aug. 2018, pp. 1–5.

[9] K. An, T. Liang, G. Zheng, X. Yan, Y. Li, and S. Chatzinotas, ''Performance limits of cognitive-uplink FSS and terrestrial FS for Ka-band,'' *IEEE Trans. Aerosp. Electron. Syst.*, vol. 55, no. 5, pp. 2604–2611, Oct. 2019.

[10] Y. Cai, Z. Qin, F. Cui, G. Y. Li, and J. A. McCann, ''Modulation and multiple access for 5G networks,'' *IEEE Commun. Surveys Tuts.*, vol. 20, no. 1, pp. 629–646, 1st Quart., 2018.

[11] H. Haci, H. Zhu, and J. Wang, ''Performance of non-orthogonal multiple access with a novel asynchronous interference cancellation technique,'' *IEEE Trans. Commun.*, vol. 65, no. 3, pp. 1319–1335, Mar. 2017.

[12] Y. Liu, Z. Qin, M. Elkashlan, Z. Ding, A. Nallanathan, and L. Hanzo, ''Nonorthogonal multiple access for 5G and beyond,'' *Proc. IEEE*, vol. 105, no. 12, pp. 2347–2381, Dec. 2017.

[13] W. Cao, Y. Zou, Z. Yang, and J. Zhu, ''Relay selection for improving physical-layer security in hybrid satellite-terrestrial relay networks,'' *IEEE Access*, vol. 6, pp. 65275–65285, 2018.

[14] T. N. Nguyen, D.-H. Tran, T. Van Chien, V.-D. Phan, M. Voznak, and S. Chatzinotas, ''Security and reliability analysis of satellite-terrestrial multirelay networks with imperfect CSI,'' *IEEE Syst. J.*, early access, Sep. 8, 2022, doi: 10.1109/JSYST.2022.3201128.

[15] V. Bankey and P. K. Upadhyay, ''Ergodic capacity of multiuser hybrid satellite-terrestrial fixed-gain AF relay networks with CCI and outdated CSI,'' *IEEE Trans. Veh. Technol.*, vol. 67, no. 5, pp. 4666–4671, May 2018.

[16] K. An and T. Liang, ''Hybrid satellite-terrestrial relay networks with adaptive transmission,'' *IEEE Trans. Veh. Technol.*, vol. 68, no. 12, pp. 12448–12452, Dec. 2019.

[17] K. An, Y. Li, X. Yan, and T. Liang, ''On the performance of cache-enabled hybrid satellite-terrestrial relay networks,'' *IEEE Wireless Commun. Lett.*, vol. 8, no. 5, pp. 1506–1509, Oct. 2019.

[18] M. R. Bhatnagar and M. K. Arti, ''Performance analysis of AF based hybrid satellite-terrestrial cooperative network over generalized fading channels,'' *IEEE Commun. Lett.*, vol. 17, no. 10, pp. 1912–1915, Oct. 2013.

[19] M. K. Arti, ''Channel estimation and detection in hybrid satellite-terrestrial communication systems,'' *IEEE Trans. Veh. Technol.*, vol. 65, no. 7, pp. 5764–5771, Jul. 2016.

[20] S. Sreng, B. Escrig, and M.-L. Boucheret, ''Exact outage probability of a hybrid satellite terrestrial cooperative system with best relay selection,'' in *Proc. IEEE Int. Conf. Commun. (ICC)*, Jun. 2013, pp. 4520–4524.

[21] K. Guo, M. Lin, B. Zhang, J.-B. Wang, Y. Wu, W.-P. Zhu, and J. Cheng, ''Performance analysis of hybrid satellite-terrestrial cooperative networks with relay selection,'' *IEEE Trans. Veh. Technol.*, vol. 69, no. 8, pp. 9053–9067, Aug. 2020.

[22] L. Yang and M. O. Hasna, ''Performance analysis of amplify-and-forward hybrid satellite-terrestrial networks with cochannel interference,'' *IEEE Trans. Commun.*, vol. 63, no. 12, pp. 5052–5061, Dec. 2015.

[23] T. N. Nguyen, L.-T. Tu, D.-H. Tran, V.-D. Phan, M. Voznak, S. Chatzinotas, and Z. Ding, ''Outage performance of satellite terrestrial full-duplex relaying networks with co-channel interference,'' *IEEE Wireless Commun. Lett.*, vol. 11, no. 7, pp. 1478–1482, Jul. 2022.

[24] X. Yue, Y. Liu, Y. Yao, T. Li, X. Li, R. Liu, and A. Nallanathan, ''Outage behaviors of NOMA-based satellite network over shadowed-rician fading channels,'' *IEEE Trans. Veh. Technol.*, vol. 69, no. 6, pp. 6818–6821, Jun. 2020.

[25] S. A. Tegos, P. D. Diamantoulakis, J. Xia, L. Fan, and G. K. Karagiannidis, ''Outage performance of uplink NOMA in land mobile satellite communications,'' *IEEE Wireless Commun. Lett.*, vol. 9, no. 10, pp. 1710–1714, Oct. 2020.

[26] X. Yan, H. Xiao, K. An, and C.-X. Wang, ''Outage performance of NOMA-based hybrid satellite-terrestrial relay networks,'' *IEEE Wireless Commun. Lett.*, vol. 7, no. 4, pp. 538–541, Aug. 2018.

[27] Z. Lin, M. Lin, J.-B. Wang, T. de Cola, and J. Wang, ''Joint beamforming and power allocation for satellite-terrestrial integrated networks with non-orthogonal multiple access,'' *IEEE J. Sel. Areas Commun.*, vol. 13, no. 3, pp. 657–670, Jun. 2019.

[28] N.-T. Nguyen, H.-N. Nguyen, N.-L. Nguyen, A.-T. Le, D.-T. Do, and M. Voznak, ''Enhancing spectrum efficiency for multiple users in hybrid satellite-terrestrial networks,'' *IEEE Access*, vol. 9, pp. 50291–50300, 2021.

[29] A.-T. Le, N.-D.-X. Ha, D.-T. Do, S. Yadav, and B. M. Lee, ''Enabling NOMA in overlay spectrum sharing in hybrid satellite-terrestrial systems,'' *IEEE Access*, vol. 9, pp. 56616–56629, 2021.

[30] V. Singh and P. K. Upadhyay, ''Exploiting FD/HD cooperative-NOMA in underlay cognitive hybrid satellite-terrestrial networks,'' *IEEE Trans. Cognit. Commun. Netw.*, vol. 8, no. 1, pp. 246–262, Mar. 2022.

[31] V. Singh and P. K. Upadhyay, ''Exploiting cache-free/cache-aided TWR-NOMA in cognitive hybrid satellite-terrestrial networks,'' *IEEE Trans. Veh. Technol.*, vol. 71, no. 2, pp. 1778–1793, Feb. 2022.

[32] X. Li, Y. Chen, P. Xue, G. Lv, and M. Shu, ''Outage performance for satellite-assisted cooperative NOMA systems with coordinated direct and relay transmission,'' *IEEE Commun. Lett.*, vol. 24, no. 10, pp. 2285–2289, Oct. 2020.

[33] L. Han, W.-P. Zhu, and M. Lin, ''Outage of NOMA-based hybrid satellite-terrestrial multi-antenna DF relay networks,'' *IEEE Wireless Commun. Lett.*, vol. 10, no. 5, pp. 1083–1087, May 2021.

[34] H. Shuai, K. Guo, K. An, and S. Zhu, ''NOMA-based integrated satellite terrestrial networks with relay selection and imperfect SIC,'' *IEEE Access*, vol. 9, pp. 111346–111357, 2021.

[35] L. Han, W.-P. Zhu, and M. Lin, ''Outage analysis of multi-relay NOMA-based hybrid satellite-terrestrial relay networks,'' *IEEE Trans. Veh. Technol.*, vol. 71, no. 6, pp. 6469–6487, Jun. 2022.

[36] M. Toka, M. Vaezi, and W. Shin, ''Outage analysis of Alamouti-NOMA scheme for hybrid satellite-terrestrial relay networks,'' *IEEE Internet Things J.*, early access, Nov. 15, 2022, doi: 10.1109/JIOT.2022.3222414.

[37] N.-T. Nguyen, H.-N. Nguyen, A.-T. Le, N. D. Nguyen, D.-T. Do, and M. Voznak, ''Impact of CCI on performance analysis of downlink satellite-terrestrial systems: Outage probability and ergodic capacity perspective,'' *EURASIP J. Wireless Commun. Netw.*, vol. 2022, no. 1, pp. 1–25, Aug. 2022.

[38] M. K. Arti and M. R. Bhatnagar, ''Beamforming and combining in hybrid satellite-terrestrial cooperative systems,'' *IEEE Commun. Lett.*, vol. 18, no. 3, pp. 483–486, Mar. 2014.

[39] D. B. D. Costa and S. Aissa, ''Cooperative dual-hop relaying systems with beamforming over Nakagami-m fading channels,'' *IEEE Trans. Wireless Commun.*, vol. 8, no. 8, pp. 3950–3954, Aug. 2009.

[40] H. Shuai, K. Guo, K. An, Y. Huang, and S. Zhu, ''Transmit antenna selection in NOMA-based integrated Satellite-HAP-Terrestrial networks with imperfect CSI and SIC,'' *IEEE Wireless Commun. Lett.*, vol. 11, no. 8, pp. 1565–1569, Aug. 2022.

[41] G. R. MacCartney, J. Zhang, S. Nie, and T. S. Rappaport, ''Path loss models for 5G millimeter wave propagation channels in urban microcells,'' in *Proc. IEEE Global Commun. Conf. (GLOBECOM)*, Dec. 2013, pp. 3948–3953.

[42] Z. Ding, Z. Yang, P. Fan, and H. V. Poor, ''On the performance of non-orthogonal multiple access in 5G systems with randomly deployed users,'' *IEEE Signal Process. Lett.*, vol. 21, no. 12, pp. 1501–1505, Dec. 2014.

[43] S. Lin, L. Zhu, Y. Guo, and X. Gou, ''Distribution characteristics and performance simulations of rain attenuation at Ka band for satellite communications,'' in *Proc. 5th Global Symp. Millim.-Waves*, May 2012, pp. 579–582.

[44] C.-Q. Dai, N.-N. Huang, and Q. Chen, ''Adaptive transmission scheme in Ka-band satellite communications,'' in *Proc. IEEE Int. Conf. Digit. Signal Process. (DSP)*, Oct. 2016, pp. 336–340.

[45] P. K. Upadhyay and P. K. Sharma, ''Max-max user-relay selection scheme in multiuser and multirelay hybrid satellite-terrestrial relay systems,'' *IEEE Commun. Lett.*, vol. 20, no. 2, pp. 268–271, Feb. 2016.
[46] I. S. Gradshteyn and I. M. Ryzhik, *Table of Integrals, Series, and Products*. New York, NY, USA: Academic, 2014.
[47] K. An, M. Lin, T. Liang, J.-B. Wang, J. Wang, Y. Huang, and A. L. Swindlehurst, ''Performance analysis of multi-antenna hybrid satellite-terrestrial relay networks in the presence of interference,'' *IEEE Trans. Commun.*, vol. 63, no. 11, pp. 4390–4404, Nov. 2015.
[48] H. A. David and H. N. Nagaraja, *Order Statistics*. Hoboken, NJ, USA: Wiley, 2004.
[49] X. Yue, Y. Liu, S. Kang, A. Nallanathan, and Y. Chen, ''Modeling and analysis of two-way relay non-orthogonal multiple access systems,'' *IEEE Trans. Commun.*, vol. 66, no. 9, pp. 3784–3796, Sep. 2018.
[50] Q. Zhang, K. An, X. Yan, and T. Liang, ''Coexistence and performance limits for the cognitive broadband satellite system and mmWave cellular network,'' *IEEE Access*, vol. 8, pp. 51905–51917, 2020.
[51] F. Guidolin, M. Nekovee, L. Badia, and M. Zorzi, ''A study on the coexistence of fixed satellite service and cellular networks in a mmWave scenario,'' in *Proc. IEEE Int. Conf. Commun. (ICC)*, Jun. 2015, pp. 2444–2449.
[52] K. An, M. Lin, J. Guyang, T. Liang, J.-B. Wang, and W.-P. Zhu, ''Outage performance for the cognitive broadband satellite system and terrestrial cellular network in millimeter wave scenario,'' in *Proc. IEEE Int. Conf. Commun. (ICC)*, May 2017, pp. 1–6.
[53] F. B. Hildebrand, *Introduction to Numerical Analysis*. Chelmsford, MA, USA: Courier Corporation, 1987.

NHAT-TIEN NGUYEN received the B.Eng. degree from the Posts and Telecommunications Institute of Technology, Ho Chi Minh City, Vietnam, and the M.Eng. degree from the Ho Chi Minh City University of Technology (HCMUT), in 2017. He is currently pursuing the Ph.D. degree in communication technology with the Technical University of Ostrava, Czech Republic. Since 2003, he has been a Senior Technician at Saigon Postel Corporation. Since 2018, he has also been a Lecturer at Saigon University. His research interests include MIMO, NOMA, D2D transmission, energy harvesting, millimeter wave communications, hybrid satellite-terrestrial networks, and wireless sensor networks.

HONG-NHU NGUYEN received the B.Sc. degree in electronics engineering from the Ho Chi Minh City University of Technology, in 1998, the M.Eng. degree in electronics engineering from the University of Transport and Communications, Vietnam, in 2012, and the Ph.D. degree in telecommunications from the VSB–Technical University of Ostrava, Czech Republic, in 2021. He is currently working as a Lecturer at Saigon University. His research interests include applied electronics, wireless communications, cognitive radio, NOMA, and energy harvesting.

NGOC-LONG NGUYEN was born in Vietnam, in 1973. He received the B.S. and M.S. degrees in electric physics from the University of Science, Vietnam, and the Ph.D. degree in telecommunications from the VSB–Technical University of Ostrava, Czech Republic, in 2021. He is currently a Lecturer with the Faculty of Applied Sciences, Ton Duc Thang University. His research interests include applied electronics, wireless communication, NOMA, cognitive radio, and energy harvesting.

ANH-TU LE (Member, IEEE) was born in Lam Dong, Vietnam, in 1997. He received the B.S. degree from the Industrial University of Ho Chi Minh City, Vietnam, in 2019, and the M.S. degree from Ton Duc Thang University, Vietnam, in 2022. He has authored and coauthored over 25 ISI-indexed journals. His research interests include wireless channel modeling, NOMA, cognitive radio, MIMO, and machine learning.

TAN N. NGUYEN (Member, IEEE) was born in Nha Trang, Vietnam, in 1986. He received the B.S. degree in electronics from the Ho Chi Minh University of Natural Sciences, in 2008, the M.S. degree in telecommunications engineering from Vietnam National University, in 2012, and the Ph.D. degree in communications technologies from the Faculty of Electrical Engineering and Computer Science, VSB–Technical University of Ostrava, Czech Republic, in 2019. He joined the Faculty of Electrical and Electronics Engineering, Ton Duc Thang University, Vietnam, in 2013, and since then he has been lecturing. His major research interests include cooperative communications, signal processing, cognitive radio, satellite, UAV, and physical-layer security.

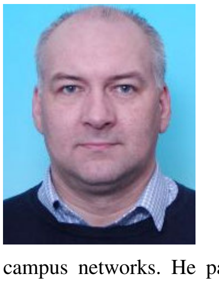

MIROSLAV VOZNAK (Senior Member, IEEE) received the Ph.D. degree in telecommunications from the Faculty of Electrical Engineering and Computer Science, VSB–Technical University of Ostrava, and the Habilitation degree, in 2009. He was appointed as a Full Professor of electronics and communications technologies, in 2017. He is a Principal Investigator in the research project QUANTUM5 funded by NATO, which focuses on the application of quantum cryptography in 5G campus networks. He participated in six projects funded by the EU in programs managed directly by European Commission. He has authored and coauthored more than 100 articles in SCI/SCIE journals. His research interests include ICT, especially on quality of service and experience, network security, wireless networks, and big data analytics. According to the Stanford University study released in 2020, he is one of the World's Top 2% of Scientists in networking and telecommunications, and information and communications technologies. He has served as the General Chair for the 11th IFIP Wireless and Mobile Networking Conference, in 2018, and the 24th IEEE/ACM International Symposium on Distributed Simulation and Real Time Applications, in 2020.